Particle Motion in Axisymmetric Stagnation Flow toward an Interface

Numerical solutions for the creeping motion of a spherical particle in a linear axisymmetric straining flow normal to a deformable interface are presented for a range of viscosity ratios, capillary numbers, and Bond numbers. The parameter ranges investigated have applications in areas of flotation (small interface deformation) and material processing (large interface deformation). The accuracy of previous solutions for flotation problems which neglect interface deformation is considered, along with the magnitude and form of interface deformation "defects" which may appear in material processing applications involving fluids containing bubbles or small particles.

J. A. Stoos and L. G. Leal
Department of Chemical Engineering
California Institute of Technology
Pasadena, CA 91125

Introduction

Many processes of great practical interest involve small particles in flowing fluids near interfaces. In polymer processing operations, these particles may be dust contaminants, an intentionally added composite reinforcing material or even very small bubbles (which behave essentially as solid particles), that are formed in the processing itself. An important problem is that these particles can lead to surface defects in the finished product of extrusion, mold filling, or coating operations, as the particles interact with the flow and the interface to produce bumps on the surface (Fritch, 1979; Hoffman, 1985). In separation processes, the particles may be mineral fines, effluent waste, or biological products that need to be removed either by flotation or by capturing the particles on a condensed film of a fibrous mat collector. Hydrodynamic interactions between the particle and interface, as well as the resulting interface deformation, may greatly affect the efficiency of capture in these cases.

In spite of the large number of applications where it is important to understand the flow-driven motion of a particle near a deformable interface, the problem has received little attention in the literature, as already observed by Hoffman. In part, this is most likely because the full nonlinear problem of a particle moving in a complicated flow near a deforming interface is difficult or impossible to solve analytically. However, the solution would also be of little general interest since nonlinearity prohibits superposition of solutions and thus restricts any results to the particular flow and geometry being investigated. However, when the particle size is small compared to the radius of curvature of the interface, a first approximation of the basic flow that forces the particle towards the interface, for both flotation (Stoos, 1987) and mold-filling operations (Hoffman, 1985), is a linear axisymmetric straining flow. Also, in coating flows it is easy to visualize from the geometries of typical coating devices (Ruschak, 1985) how extensional flow components might arise. Thus, as a first step to understanding the complicated interactions among the particle, the flow field, and the interface deformation, we investigate the basic problem of a spherical particle moving towards a deforming fluid interface under the action of a linear axisymmetric straining flow. Specifically, for application to separation processes, we would like to know how the interface deformation affects the rate of change of the minimum gap between the particle and interface, and thus how the deformation affects the capture process. For polymer processing applications, we are interested primarily in the degree and character of the interface deformation, which indicates the magnitude of possible surface defects.

The related problems of a sphere approaching a deforming fluid interface under the action of an external force (gravity) or at a constant velocity have been studied extensively, and comprehensive reviews are given by Jeffreys and Davies (1971) and Geller et al. (1986). In comparison, the problem of sphere motion driven by a flow field has received little attention and many questions remain unanswered. For instance, applications in flotation have relied on the assumption that interface deformation is negligible because of the small capillary numbers associated with the small bubble sizes (Jameson et al., 1977). However, allowing even slight deformation would relax the

The present address of J. A. Stoos is Mobil Research and Development Corporation, Paulsboro, NJ 08066.

physically unrealistic singular resistance experienced by a sphere as it approaches a nondeforming interface (usually compensated in particle capture theories by the faster singular growth of molecular attractive forces). Also, interface deformation may not be small on the scale of the small particles and certainly should not be small on the length scale of molecular attractive forces. Thus interface deformation may lead to larger separation distances when the particle approach velocity is at a minimum, and therefore to much larger approach and film thinning times. For the cases where interface deformation is neglected, bipolar coordinate solutions have been used for spheres near gas/fluid interfaces (Dukhin and Rulev, 1977), and asymptotic solutions for large separations have been developed for spheres and slender bodies near interfaces of arbitrary viscosity ratio (Yang and Leal, 1984; Stoos, 1987). In the one case where interface deformation was included, Hoffman (1985) studied the flow-driven approach of a sphere toward a deformable free interface, both theoretically and experimentally. However, his theoretical analysis involves a number of *ad hoc* assumptions and is based on the presumed existence of a rate-limiting step or quasiequilibrium configuration so that the full evolutionary problem of interface shape and sphere position is not solved.

It is, of course, well known that the interface shape and other features of the flow at any instant depend on the configuration and flow at earlier times. Thus, in general, we must investigate the entire process of sphere motion normal to the interface, starting from an initial state in which the sphere is far from the interface, which exists in its undisturbed state. Indeed, this may be especially important in the present problem because the driving force for particle motion varies with particle position and will be sensitive to any assumed configuration.

Problem Statement

We consider a spherical particle of radius a approaching normal to a deformable interface along the axis of symmetry of a linear biaxial extensional flow, starting with the sphere far from the undeformed interface. In terms of cylindrical coordinates (r, z) centered at the intersection of the axis of symmetry and the plane of the undeformed interface, the sphere center is located at $(0, l)$ and the undisturbed extensional flow has the form $u_\infty = G(ri_r - 2zi_z)$ in both fluids, where G is the strain rate. The nomenclature and particle/interface configuration is shown in Figure 1. The spherical particle is immersed entirely in the lower fluid (fluid 2), which has viscosity μ_2 and density ρ_2. The upper fluid is characterized by viscosity μ_1 and density ρ_1. The interface is characterized by a constant surface tension σ. The particle is assumed to be neutrally buoyant with density ρ_2, although nonneutrally buoyant particles could easily be considered.

The small velocities resulting from the small size of "collection" bubbles in effluent flotation and the high viscosities characteristic of polymer processing operations often allow the fluid and particle inertia to be neglected. Thus, we assume

$$Re = \frac{Ga^2\rho_2}{\mu_2} \ll 1. \tag{1}$$

Furthermore, the particle-interface separation is restricted to moderate values, i.e., less than five particle radii. In part, this is because the approximations of a planar interface and an axisymmetric extensional undisturbed flow break down at large separations in the "applications" that motivate our work. However, the particle-interface interaction also becomes increasingly unimportant for large separations. Since the particle is force-free, the slowest decaying singularity that characterizes the disturbance flow is a "stresslet" (Chwang and Wu, 1975; Yang and Leal, 1984), for which the velocity decays like $(1/l^2)$. Even though the particle velocity increases like (l), the resulting disturbance velocity is thus $O(1/l)$ or smaller at the interface and is unimportant for large separations. The relative insignificance of the disturbance flow at large separations is seen in both the asymptotic and bipolar analytic solutions for a flat interface. Later we will discuss the effects of the initial position of the sphere in more detail.

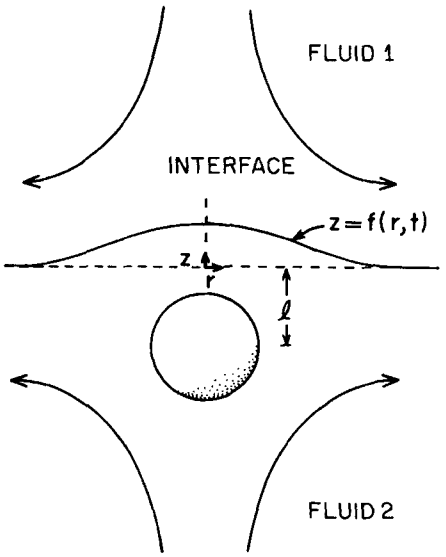

Figure 1. Schematic of problem.

Although the governing flow equations are linear, the problem is nonlinear in the boundary conditions because of the unknown interface shape and the influence of this shape on the flow. An excellent method of solution for this type of free boundary problem is the boundary integral method used by Youngren and Acrivos (1975, 1976), Geller et al. (1986), Lee and Leal (1982), and Chi and Leal (1988) among others.

Nondimensionalizing with characteristic velocity Ga, length a, and stress $\mu_2 G$, the governing flow and continuity equations for the two fluids become:

$$\left.\begin{aligned} 0 &= -\nabla p_1 + \lambda\nabla^2 u_1 \\ 0 &= \nabla \cdot u_1 \end{aligned}\right\} \quad \text{in fluid 1} \tag{2}$$

$$\left.\begin{aligned} 0 &= -\nabla p_2 + \nabla^2 u_2 \\ 0 &= \nabla \cdot u_2 \end{aligned}\right\} \quad \text{in fluid 2} \tag{3}$$

$$u_1, u_2 \to u_\infty \quad \text{as} \quad |x| \to \infty \tag{4}$$

and the boundary conditions at the interface are

$$u_1 = u_2 \tag{5}$$

$$\lambda \boldsymbol{n} \cdot \boldsymbol{T}_1 - \boldsymbol{n} \cdot \boldsymbol{T}_2 = -\frac{1}{Ca}(\nabla \cdot \boldsymbol{n})\boldsymbol{n} + \frac{1}{Cg} f \boldsymbol{n} \tag{6}$$

$$(\boldsymbol{n} \cdot \boldsymbol{u}_1)\boldsymbol{n} = (\boldsymbol{n} \cdot \boldsymbol{u}_2)\boldsymbol{n} = \left(\frac{\partial f}{\partial t}\right) \boldsymbol{i}_z + \left(\frac{\partial r}{\partial t}\right) \boldsymbol{i}_r. \tag{7}$$

Boundary conditions 5, 6 and 7 are continuity of velocity, the stress balance, and the kinematic condition for the interface motion, respectively. Here, as in Lee and Leal (1982), the interface shape is represented by $z = f(r, t)$ and the outward pointing normal at the interface is $\boldsymbol{n} \equiv \nabla H / |\nabla H|$, where $H = z - f(r, t)$. Since the driving force for sphere motion diminishes and may even change sign as the sphere approaches and crosses the plane of the undeformed interface, the interface deformation is expected to be moderate, and a more complicated multiple coordinate representation of the interface shape is not required (cf. Geller, et al., 1986).

The relevant independent dimensionless parameters are the viscosity ratio $\lambda = \mu_1/\mu_2$, the capillary number $Ca = \mu_2 Ga/\sigma$, and $Cg = \mu_2 G/ag(\rho_2 - \rho_1)$, which is the ratio of capillary to bond numbers. Ca is the ratio of characteristic viscous forces in the lower fluid to capillary forces. The parameter, Cg, is the ratio of characteristic viscous forces in the lower fluid to forces arising from the density difference between the fluids, which also tend to resist interface deformation.

The final conditions are the no-slip boundary condition on the sphere and the force balance on the sphere. The no-slip condition on the sphere surface can be expressed in the form

$$\boldsymbol{u}_2 = u_p \boldsymbol{i}_z \quad \text{at} \quad x \in S_p, \tag{8}$$

where u_p is the unknown particle velocity. The force balance on the sphere after performing an azimuthal integration yields

$$\int_0^{\pi} T^p_{nz} \sin\theta \, d\theta = 0, \tag{9}$$

where T^p_{nz} is the stress component on the particle surface in the z direction, i.e., $\boldsymbol{i}_z \cdot (\boldsymbol{n} \cdot \boldsymbol{T}^p)$.

The boundary integral method for an unbounded domain requires that the flow variables decay to zero at infinity. Therefore, the velocity and stress are written in terms of disturbance variables as in Rallison and Acrivos (1978), where $\boldsymbol{u}' \equiv \boldsymbol{u} - \boldsymbol{u}^{\infty}$ is the disturbance velocity and $\boldsymbol{T}' \equiv \boldsymbol{T} - \boldsymbol{T}^{\infty}$ is the disturbance stress. Ladyzhenskaya's general solution for the disturbance velocity and disturbance pressure at any point x is

$$\boldsymbol{u}'(x) = \frac{1}{8\pi} \int_S \left(\frac{\boldsymbol{I}}{R} + \frac{(x-\eta)(x-\eta)}{R^3}\right) \cdot \boldsymbol{T}'(\eta) \cdot \boldsymbol{n} \, dS_\eta - \frac{3}{4\pi} \int_S \frac{(x-\eta)(x-\eta)(x-\eta)}{R^5} \cdot \boldsymbol{u}'(\eta) \cdot \boldsymbol{n} \, dS_\eta \tag{10}$$

$$p'(x) = \frac{1}{2\pi} \int_S \left(\frac{\boldsymbol{I}}{R^3} - \frac{3(x-\eta)(x-\eta)}{R^5}\right) \cdot \boldsymbol{u}'(\eta) \cdot \boldsymbol{n} \, dS_\eta + \frac{1}{4\pi} \int_S \frac{(x-\eta)}{R^3} \cdot \boldsymbol{T}'(\eta) \cdot \boldsymbol{n} \, dS_\eta. \tag{11}$$

where η represents the position of points on the boundaries, S, of the flow domain, and $R \equiv |x - \eta|$. For a finite closed boundary, the above equations can be conveniently represented in terms of the actual velocity and stress, u, T, by analytically integrating out the contribution from the flow at infinity, as in Rallison and Acrivos (1978). However, for the unbounded problem considered here, this is not possible because the interface extends to infinity, where the flow strength becomes singular. Nevertheless, it is convenient to express the contributions over the particle surface in terms of the actual velocity and stress and the velocity and stress arising from the undisturbed flow field, rather than in terms of the disturbance variables.

The details of applying the boundary conditions to Eq. 10 to derive a system of integral equations for the unknown velocity and stress components at the interface and at the particle surface are similar to the constant velocity case of Lee and Leal (1982), but with additional terms in the equations from the flow at infinity. After applying the double-layer jump condition (cf. Lee and Leal, 1982), the velocity on the interface in the limit as $x \to S_I$ from fluid 2 is given by

$$\begin{aligned}\frac{1}{2}\boldsymbol{u}^{I}(x) = &-\frac{3}{4\pi}\int_{S_I}\left[\left(\frac{\boldsymbol{rrr}}{R^5}\right)\cdot\boldsymbol{u}^{I}\right]\cdot\boldsymbol{n}\,dS \\ &+\frac{1}{8\pi}\int_{S_I}\left[\left(\frac{\boldsymbol{I}}{R}+\frac{\boldsymbol{rr}}{R^3}\right)\cdot\boldsymbol{T}_2^{I}\right]\cdot\boldsymbol{n}\,dS \\ &+\frac{1}{8\pi}\int_{S_P}\left[\left(\frac{\boldsymbol{I}}{R}+\frac{\boldsymbol{rr}}{R^3}\right)\cdot\boldsymbol{T}^{P}\right]\cdot\boldsymbol{n}\,dS \\ &+\frac{3}{4\pi}\int_{S_P}\left[\left(\frac{\boldsymbol{rrr}}{R^5}\right)\cdot\boldsymbol{u}_{\infty}\right]\cdot\boldsymbol{n}\,dS \\ &-\frac{1}{8\pi}\int_{S_P}\left[\left(\frac{\boldsymbol{I}}{R}+\frac{\boldsymbol{rr}}{R^3}\right)\cdot\boldsymbol{T}_{\infty}^{P}\right]\cdot\boldsymbol{n}\,dS.\end{aligned} \tag{12}$$

The velocity on the sphere surface including the double-layer

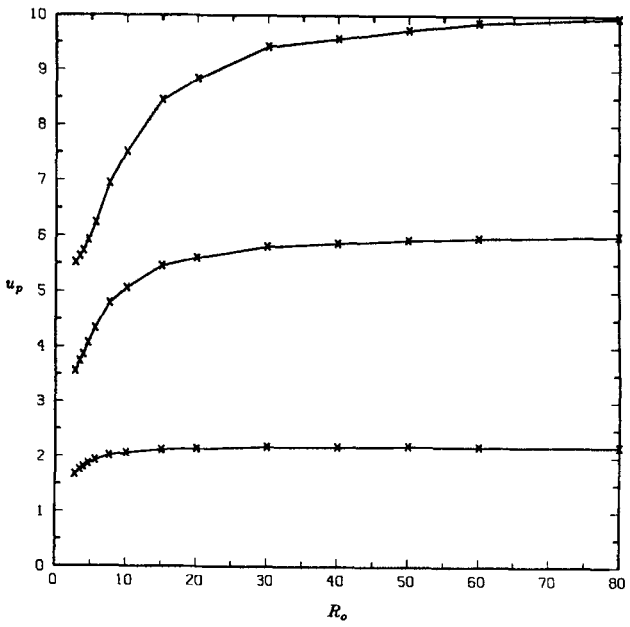

Figure 2. Effect of interface truncation on sphere velocity.

$\lambda = Ca = Cg = 1$; fixed sphere positions $l = -1.1, -3$, and -5.

jump condition is given by

$$\boldsymbol{u}^P(x) = -\frac{3}{4\pi}\int_{S_I}\left[\left(\frac{\boldsymbol{rrr}}{R^5}\right)\cdot\boldsymbol{u}^{I'}\right]\cdot\boldsymbol{n}\,dS + \frac{1}{8\pi}\int_{S_I}\left[\left(\frac{\boldsymbol{I}}{R}+\frac{\boldsymbol{rr}}{R^3}\right)\cdot\boldsymbol{T}_2^{I'}\right]\cdot\boldsymbol{n}\,dS + \frac{1}{8\pi}\int_{S_P}\left[\left(\frac{\boldsymbol{I}}{R}+\frac{\boldsymbol{rr}}{R^3}\right)\cdot\boldsymbol{T}^P\right]\cdot\boldsymbol{n}\,dS + \frac{1}{2}\boldsymbol{u}_\infty + \frac{3}{4\pi}\int_{S_P}\left[\left(\frac{\boldsymbol{rrr}}{R^5}\right)\cdot\boldsymbol{u}_\infty\right]\cdot\boldsymbol{n}\,dS - \frac{1}{8\pi}\int_{S_P}\left[\left(\frac{\boldsymbol{I}}{R}+\frac{\boldsymbol{rr}}{R^3}\right)\cdot\boldsymbol{T}_\infty^P\right]\cdot\boldsymbol{n}\,dS. \tag{13}$$

Following the example of Lee and Leal, the stress jump (Eq. 6) is incorporated by combining Eq. 12 with the similar expression for the velocity on the interface as $x \to S_I$ from fluid 1, and using the condition (Eq. 5) to obtain

$$\frac{1}{2}(\lambda+1)\boldsymbol{u}^{I'}(x) = -\frac{3}{4\pi}(1-\lambda)\int_{S_I}\left[\left(\frac{\boldsymbol{rrr}}{R^5}\right)\cdot\boldsymbol{u}^{I'}\right]\cdot\boldsymbol{n}\,dS + \frac{1}{8\pi}\int_{S_P}\left[\left(\frac{\boldsymbol{I}}{R}+\frac{\boldsymbol{rr}}{R^3}\right)\cdot\boldsymbol{T}^P\right]\cdot\boldsymbol{n}\,dS - \frac{1}{8\pi}\int_{S_I}\left[\left(\frac{\boldsymbol{I}}{R}+\frac{\boldsymbol{rr}}{R^3}\right)\cdot\boldsymbol{F}'(f)\right]\cdot\boldsymbol{n}\,dS + \frac{3}{4\pi}\int_{S_P}\left[\left(\frac{\boldsymbol{rrr}}{R^5}\right)\cdot\boldsymbol{u}_\infty\right]\cdot\boldsymbol{n}\,dS - \frac{1}{8\pi}\int_{S_P}\left[\left(\frac{\boldsymbol{I}}{R}+\frac{\boldsymbol{rr}}{R^3}\right)\cdot\boldsymbol{T}_\infty^P\right]\cdot\boldsymbol{n}\,dS. \tag{14}$$

The disturbance stress difference F' is given by

$$\boldsymbol{F}' \equiv (\lambda\boldsymbol{n}\cdot\boldsymbol{T}_1^I - \boldsymbol{n}\cdot\boldsymbol{T}_2^I - (\lambda\boldsymbol{n}\cdot\boldsymbol{T}_{1\infty}^I - \boldsymbol{n}\cdot\boldsymbol{T}_{2\infty}^I), \tag{15}$$

where in cylindrical coordinates (r, θ, z), the stress associated with the undisturbed flow and the flat interface is

$$\boldsymbol{T}_{2\infty}^I = -p_{2\infty}\boldsymbol{I} + \begin{pmatrix}2&0&0\\0&0&0\\0&0&-4\end{pmatrix},$$

$$\boldsymbol{T}_{1\infty}^I = -p_{1\infty}\boldsymbol{I} + \begin{pmatrix}2&0&0\\0&0&0\\0&0&-4\end{pmatrix}, \tag{16}$$

and $p_{2\infty}\,p_{1\infty}$ are constants that must satisfy the normal stress balance on a flat interface with the velocity field $\boldsymbol{u}_\infty$:

$$\boldsymbol{n}\cdot(\lambda\boldsymbol{n}\cdot\boldsymbol{T}_{1\infty}^I - \boldsymbol{n}\cdot\boldsymbol{T}_{2\infty}^I) = p_{2\infty} - \lambda p_{1\infty} + 4(1-\lambda) = 0. \tag{17}$$

A solution of Eq. 17 is $p_{2\infty} = p_{1\infty} = -4$. The dynamic pressure from the undisturbed flow is negative (the hydrostatic pressure jump across a flat interface is identically zero) and balances the viscous stress, which would tend to move the interface from a nonequilibrium position in a situation with unequal fluid viscosities.

The integral equations (Eqs. 9 and 12–14) can be solved simultaneously to determine the unknown velocity and stress components on the interface and particle surface, u^I, T_2^I, T^P and u_p, assuming that the shape function $f(r)$ is specified. In this case, the disturbance stress difference is known,

$$\boldsymbol{F}'(f) = -\frac{1}{Ca}\left(\frac{\kappa}{r}\frac{\partial f}{\partial r} + \kappa^3\frac{\partial^2 f}{\partial r^2}\right)\boldsymbol{n} + \frac{1}{Cg}f\boldsymbol{n} + 6(\lambda-1)(\boldsymbol{n}\cdot\boldsymbol{i}_r)\boldsymbol{i}_r, \tag{18}$$

as well as

$$\boldsymbol{T}_\infty = 6(\boldsymbol{n}\cdot\boldsymbol{i}_r)\,\boldsymbol{i}_r, \tag{19}$$

and

$$\boldsymbol{u}_\infty = (r\boldsymbol{i}_r - 2z\boldsymbol{i}_z). \tag{20}$$

The last term in Eq. 18, which depends on λ, is the stress difference arising from the undisturbed flow at infinity and is zero for a flat interface or for two fluids of equal viscosity. The only condition of the original problem that is not built into the system of equations above is the kinematic condition (Eq. 7), and this condition is used with the known interface velocity u^I to update the interface shape function, as described in the next section. The surface integrals in Eqs. 12–14 are reduced to line integrals by integrating out the azimuthal dependence for this axisymmetric problem.

Numerical Algorithm

The method of solution is a numerical collocation scheme, similar to that used by Geller et al. (1986). The infinite interface boundary is truncated at some large but finite radius, R_o, and is subdivided, along with the particle surface, into N_I and N_P small segments, respectively. The number of segments used varied between 25–35 unequal sized segments for N_I, with the highest concentration of segments near the particle where the interface deformation is largest and 15–25 evenly spaced segments for N_P. The unknown basis functions for the velocity and stress are assumed to vary linearly over these small segments. Alternatively, high accuracy could also be maintained by increasing the number of boundary elements and using constant basis functions over the elements (cf. Lee and Leal, 1982; Youngren and Acrivos, 1975, 1976). However, the use of linear basis functions is numerically faster than increasing the number of boundary elements. Vector equations (Eqs. 12 and 14) are evaluated at the N_I interface interval centers, and vector equation (Eq. 13) is evaluated at the N_P particle interval centers, thus generating a system of $4N_I + 2N_P$ linear algebraic equations (Kantorovich and Krylov, 1958). Including the force balance on the particle, Eq. 9, we have $4N_I + 2N_P + 1$ equations to solve for the $4N_I + 2N_P + 1$ unknowns: $u_r^I(N_I)$, $u_z^I(N_I)$, $T_{2nr}^I(N_I)$, $T_{2nz}^I(N_I)$, $T_{nr}^P(N_P)$, $T_{nz}^P(N_P)$ and u_p.

The normal vector to the interface and the local interface curvature, which appear in the integrands of Eqs. 12–14, are evaluated using a cubic spline to represent the interface shape in terms of a function $f(r)$. For cases with large interface deformation, the cylindrical coordinate representation $f(r)$ is replaced by a parameterization in terms of arc length s, and cubic splines are fit to both $f(s)$ and $r(s)$; however, this method is somewhat slower and thus is not used if the deformation is not large: i.e., $df/dr < 10$. The azimuthal integration reduces the surface integrals to line integrals with integrands involving elliptic integrals (Lee and Leal, 1982). These final line integrals are evaluated numerically using a seven-point Gaussian quadrature, and the accuracy is checked by occasionally comparing to an 11-point Gaussian quadrature. In performing this integration, a small line element is cut out around the singular point and evaluated analytically. In addition, the accuracy is improved by further subdividing the main element into smaller elements near the singular points. Once the interface and sphere velocities have been evaluated, the interface shape is allowed to evolve by explicitly stepping the position of each of the node points on the interface with the normal velocity at that node point. Since the actual node point position is important only as it relates to the description of the interface shape, convection of the node points tangent to the interface is not of interest. Furthermore, restriction of nodes to normal motion reduces the depletion of node points near the particle. Nevertheless, some spreading of node points does still occur, and thus, periodically, the points are redistributed using the cubic spline to maintain the initial spacing. Similarly, the sphere position is changed by $u_p \Delta t$.

A sufficiently small time step is used so that relative changes in velocity at each time step are small. If the change in velocity is relatively large (greater than 5%) either at a node point on the interface or for the particle, the evolution is stopped and restarted from a previous point in time, using a smaller time step. The initial nondimensional time step used was 0.01, (nondimensionalized with characteristic time G^{-1}), which is somewhat smaller than that in Geller et al. (1986), since the initial sphere velocity is larger, thus producing larger relative changes in the particle-interface configuration. Adjusting the time step to maintain small changes in velocities results in smaller time steps for smaller particle/interface separations, since at this point small changes in position produce large relative changes in particle/interface separation and thus large relative changes in particle velocity. The smallest time step used was 0.0001. If smooth changes in velocity were not achieved with this time step, the calculation was stopped.

The effects of the interface truncation are shown in Figure 2. Because the flow disturbance due to the particle is convected radially by the undisturbed flow, the interface truncation distance must be substantially larger than in the constant force case of Geller et al. (1986). Similar to the latter case, however, the truncation distance must be increased as the particle/interface separation becomes larger. However, for separation distances of 3.0 (from the particle center), the sphere velocity in the present case is insensitive to truncation distances for R_o of 30.0 or more. In addition, the disturbance velocity and stress on the interface at $R_o = 30$ are both less than $5 \cdot 10^{-4}$.

The effect of the initial starting position is shown in Figure 3, where interface shapes are plotted for $Ca = Cg = \lambda = 1$, with starting positions of 3 and 5, and an initially flat interface. Initially the starting position can affect the interface shape and the

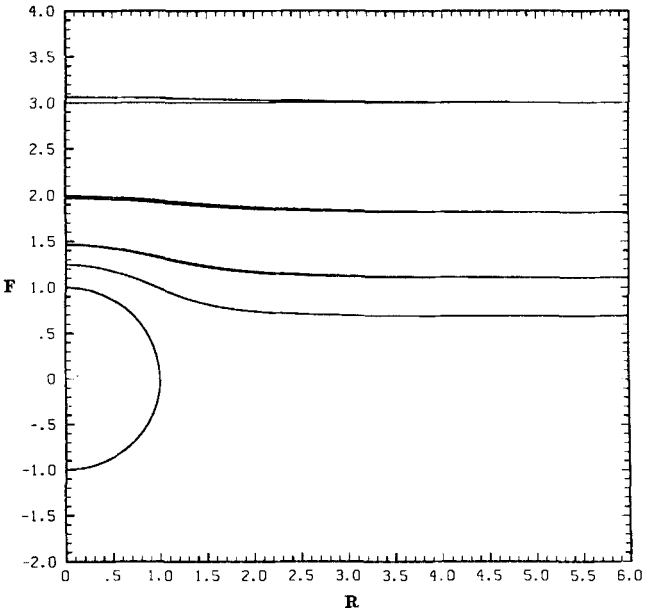

Figure 3. Effect of sphere starting position on interface shape.

Initial starting positions, $l_o = -3$ and -5, $\lambda = Ca = Cg = 1$; dimensionless time between contours $\Delta t_c = 0.25$.

sphere velocity; since the interaction is small at large separations, however, the interface remains nearly flat in either case. As we will show later, the sphere velocity for large separations, is very close to the results for a flat (but deforming) interface, so the effect of this small change in interface shape on the sphere velocity is small. As the separation decreases, the interface shapes and sphere velocities agree more closely for the two cases. Thus, the major characteristics of the solutions for identical Ca, Cg and λ are insensitive to the initial starting position as long as it is not too small. An initial separation of 3 was used in all the subsequent calculations.

Limiting Cases of Small Deformation

In this section, we present results from our calculations for various combinations of the dimensionless parameters. The results divide nicely into two quite distinct groups. In the first set, we briefly consider cases involving a large viscosity ratio, or very small values of Ca or Cg, in which the interface deformation is small. The solutions in this case are presented, in part, as an indication of the accuracy and reliability of the numerical technique. However, the results are also of some direct interest in the context of particle capture in flotation processes, where Ca and Cg are typically very small, and the interface deformation is also small. Following this, we consider a second set of results for $0.1 \leq Ca, Cg \leq 10.0$, and $0.0 \leq \lambda \leq 10.0$, where interface deformation is large. These results are of more direct interest in materials processing applications, as discussed earlier, where an understanding of the deformation process and the factors that control it is important in controlling the magnitude of surface bumps or defects in products produced using particle- or bubble-filled molten materials. In the latter case, we compare the results from our computations with experimental observations from the study of Hoffman (1985).

We begin by considering cases involving a large viscosity ratio

($\lambda \gg 1$) or weak viscous forces (i.e., Ca, $Cg \ll 1$), where interface deformation is small. The *limiting* cases of small capillary number or large viscosity ratios are of special interest in the context of particle capture in the flotation process, where the corresponding approximation of a *flat* nondeforming interface, ($u \cdot n = 0$), has formed the basis of existing theoretical models and predictions of capture efficiency. However, it seems evident that the occurrence of even a small amount of interface deformation accompanying the approach of a small particle toward the bubble surface may be an important factor in the capture process, which relies on nonhydrodynamic, but extremely short-range attractive forces, in its final stages. It is particularly interesting, in this regard, to compare results from the present numerical scheme, with the limiting, flat-interface analytical results. The two most important points for comparison are the minimum gap width between the particle and the interface as a function of time, and the position of the particle relative to the plane of the undeformed interface (the latter controls the magnitude of the *tangential* velocity of a particle as it passes around the bubble, and thus also controls the time (sliding time) available for thinning of the minimum gap between the particle and the interface to a point where capture is possible (c.f. Dobby and Finch, 1985, where sliding times for the intermediate Reynolds number case are considered).

The related problem of small deformation accompanying the approach of a sphere towards an interface at constant velocity was investigated by Berdan and Leal (1982), using a domain perturbation technique. However, this type of analytic approach has limited value for analysis of the effect of interface deformation on particle capture, because tractable analytic forms for the velocity and pressure fields are possible only in the limit of a *large* separation between the sphere and the interface, where the method of reflections can be employed along with "simple" solutions based on a superposition of fundamental singularities at the sphere center. Theories for the opposite limit of "lubrication-like" film drainage rely on either input of an initial "shape" for the film from experimental (or other) evidence, or on "ad hoc" approximations.

In the present section, we consider numerical results for two cases: first, $\lambda = 0$ and small $Ca = Cg = 0.01$, which is "representative" of conditions for flotation processes; and second, $Ca = Cg = 1$ with $\lambda = 100$, which provides a comparison in which interface deformation is very small because of dominant viscous effects.

Results showing the interface shape for these two cases are presented in Figures 4 and 5, where for clarity of presentation, we adopt a frame of reference in which the particle appears to be fixed, with the interface approaching it, starting from an initial configuration in which the interface is flat and located three radii away from the center of the sphere. The interface in these figures is pictured at equal time intervals (0.25 nondimensional time units) so that the contours become closer together as the sphere slows down because of the combined effects of hydrodynamic interaction with the interface and a decrease in the undisturbed fluid velocity for positions that are closer to the interface.

The most striking feature of the results shown in Figures 4 and 5 is that the degree of interface deformation is almost imperceptible with the scale of resolution that is inherent in these figures, until the sphere is extremely close to the plane of the undeformed interface. Indeed, in order to provide a useful

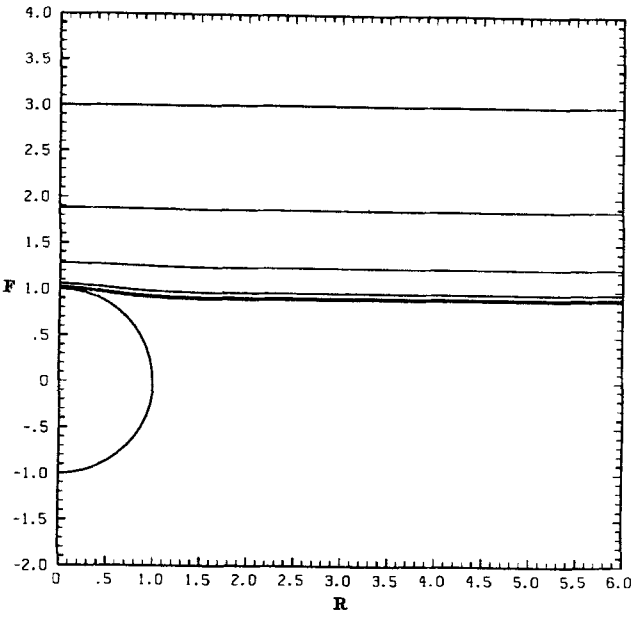

Figure 4. Interface shape as a function of sphere position: $\lambda = 0$; $Ca = Cg = 0.01$; $l_o = -3$, $\Delta t_c = 0.25$.

view of the actual shape of the thin fluid region for the last few time steps in Figures 4 and 5, we reproduce an expanded local view of both of these thin films in Figure 6 at times 1.25 and 1.0, respectively.

The very small deformation in the present case for $Ca = Cg = 0.01$ and $\lambda = 0.0$ may be contrasted with the earlier predictions of Geller et al. (1986) for a sphere approaching an interface through a quiescent fluid under the action of a constant force. In the latter case, considerable deformation occurred for Ca, $Cg = O(10^{-2})$. Indeed, to restrict the interface to a nearly flat shape, comparable qualitatively with that shown in Figures 4 and 5, it

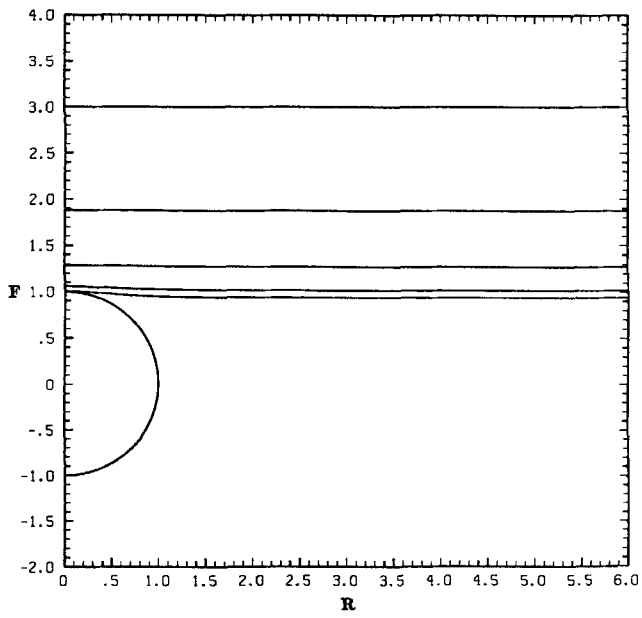

Figure 5. Interface shape as a function of sphere position: $\lambda = 100$; $Ca = Cg = 1$; $l_o = -3$; $\Delta t_c = 0.25$.

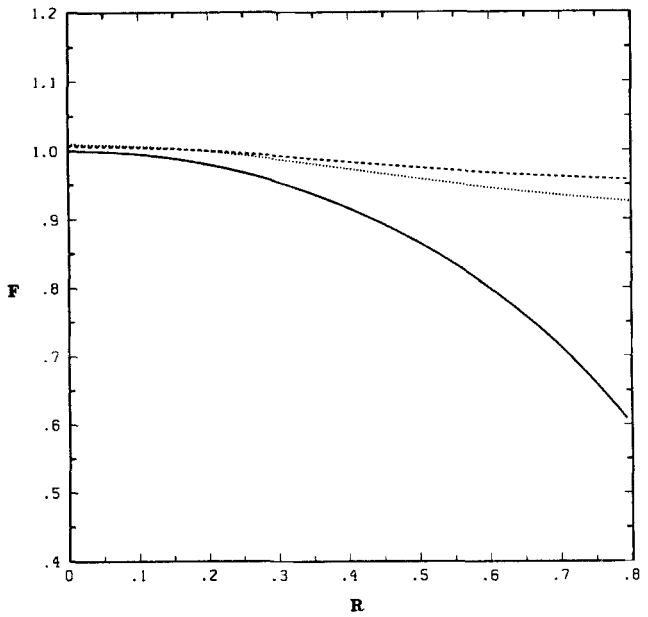

Figure 6. Expanded view of thin film regions in Figures 4 and 5.

———, sphere surface; ----- $\lambda = 0$, $Ca = Cg = 0.01$; · · · · ·, $\lambda = 100$, $Ca = Cg = 1$.

was necessary to reduce Ca and/or Cg by another order of magnitude. We shall see that the degree of deformation in the present case is always considerably smaller for equal values of the dimensionless parameters, λ, Ca and Cg than that predicted by Geller et al. (1986) for motion under the action of a constant force.

There are at least three reasons for this conclusion:

1. The magnitude of the undisturbed velocity in the present case decreases linearly with distance from the plane of the undeformed interface. Hence, the velocity of the particle will decrease as the interface is approached (and would do so in the complete absence of any hydrodynamic interactions with the interface) and the magnitude of viscous deforming forces will likewise decrease. It is noteworthy in this regard that the characteristic velocity inherent in Ca and Cg is the velocity of the undisturbed flow at a distance of one sphere radius from the interface, whereas the characteristic velocity used by Geller et al. was the Stokes velocity for a sphere moving at very large distances from the interface under the action of the applied force.

2. The disturbance flow produced by the sphere is much "weaker." In particular, since the particle is force- and torque-free, the disturbance velocity produced by the particle decays like a force dipole (in particular, a "stresslet") proportional to $1/l^2$, rather than a point force (or "Stokeslet") proportional to $1/l$ as in the earlier studies. This results in smaller disturbance effects and less deviation of the particle velocity from the undisturbed fluid velocity for large particle/interface separations.

3. The undisturbed flow field tends to maintain the interface in a flat configuration. This effect is inherent in both the form of the undisturbed flow field (which is added to the disturbance velocity in calculating the net velocity of the interface) and in the last term of the normal stress difference given by Eq. 18, which act together as a "restoring" force that will cause an initially deformed interface to return to a flat configuration even in the absence of interfacial tension or a density jump across the interface (i.e., for $Ca = Cg = \infty$). An explicit computational demonstration of this latter fact will be given in the next section, where we consider large amplitude deformations.

As indicated in the introduction to this section, the most important characteristic for the small deformation problems considered here is not the overall interface shape, but rather the time-dependent thickness of the thin film that eventually appears between the sphere and the interface, and the position of the sphere relative to the plane of the undeformed interface. These factors are explored in Figure 7 for the "flotation" parameters (i.e., $Ca = Cg = 0.01$, $\lambda = 0$). For the present "exact" numerical solution, we plot both the minimum distance of the surface of the sphere from the plane $z = 0$, and the minimum thickness of the thin liquid film. Also shown, for comparison, are predictions of the minimum film thickness for a flat interface via the asymptotic (far-field) solution of Yang and Leal (1984), and the bipolar coordinate solution of Dukhin and Rulev (1977).

4. Superficially, the various curves in Figure 7 look very similar; indeed, the importance of the differences depends on the critical film thickness for capture (i.e, the gap width at which nonhydrodynamic forces of attraction become sufficiently strong to cause the thin film to rupture (Derjaguin and Duklin, 1979). For example, the time for the sphere/interface gap to decrease below 0.01 of the particle radius is almost twice that predicted by the far-field result of Yang and Leal (1984). The bipolar solution of Dukhin and Rulev is much closer to the exact solution for these particular values of Ca and Cg, but still slightly underestimates the minimum film thickness at any instant in time. The bipolar solution also overestimates slightly the position of the sphere relative to the plane $z = 0$. Although both errors are relatively small in absolute terms, they may cause significant errors in the full flotation capture calculations.

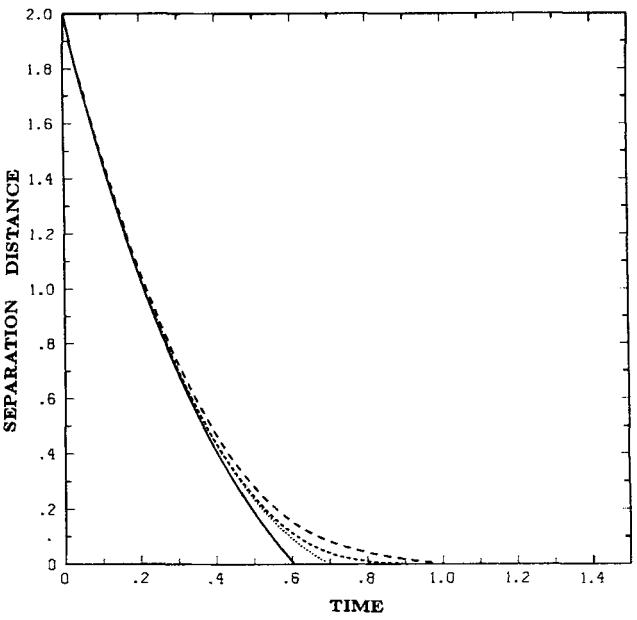

Figure 7. Particle position and minimum "film" thickness as a function of time for $Ca = Cg = 0.01$, $\lambda = 0$.

———, far-field asymptotic result for a flat interface; -----, bipolar coordinate result for a flat interface; · · · · ·, boundary integral result for particle position relative to $z = 0$; — —, boundary integral result for the minimum thickness of the thin liquid film.

The error in the position of the particle relative to the plane $z = 0$ will significantly affect the tangential velocity of the particle (Stoos, 1987), and this in turn may affect whether or not the particle is predicted to have sufficient time in the extensional flow near the interface to reach a critical film thickness for capture.

Another, more sensitive, comparison between the present numerical results and previous analytic theories for a flat interface is shown in Figure 8. Here, we plot the *ratio* of the particle velocity to the velocity of the undisturbed flow field at the particle center—we shall refer to this as the "relative" velocity. The results from our present solution for $Ca = Cg = 0.01$ and $\lambda = 0$ are plotted both as a function of particle position relative to the plane $z = 0$ and as a function of particle position relative to the interface. Results are also shown for the far-field asymptotic and bipolar coordinate solutions for a flat, nondeforming interface and for a flat, but *deforming*, interface via a supplemental boundary integral calculation. The particle velocity as a function of particle position relative to the plane $z = 0$ is significantly larger for the deformed interface than the particle velocity given for a flat, nondeforming interface by the bipolar coordinate solution, since the allowance of even a small amount of interface deformation reduces the resistance to the particle approach. However, the particle velocity as a function of particle position relative to the interface agrees quite well with the bipolar coordinate solution for *no* deformation.

From this, we conclude that interface deformation affects the particle velocity principally by changing the minimum separation between the particle and the interface, rather than as a consequence of changes in the interface shape directly. The velocity

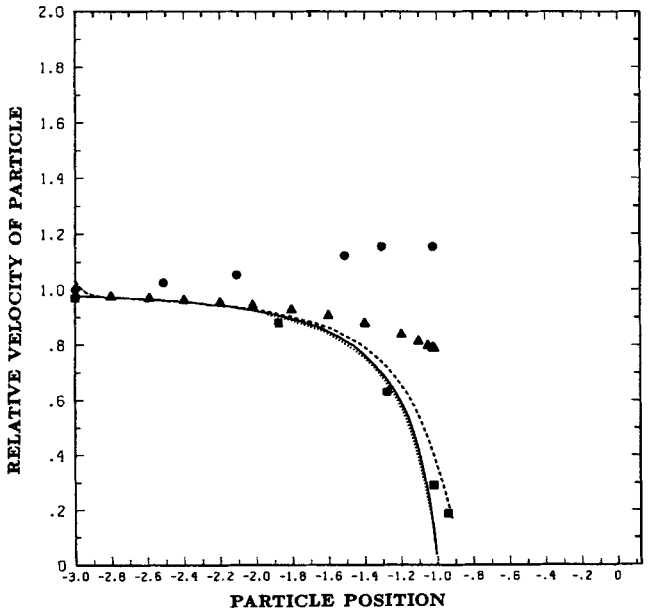

Figure 8. Relative velocity of the particle as a function of particle position for $Ca = Cg = 0.01$, $\lambda = 0$.

———, bipolar coordinate solution for a flat, nondeforming interface; -----, boundary integral solution as a function of particle position relative to $z = 0$; · · · · ·, boundary integral solution as a function of particle position relative to the deformed interface; Δ, far-field asymptotic solution for a flat nondeforming interface; O, boundary integral solution as a function of particle position relative to $z = 0$ for a flat but deforming interface. Also shown, for comparison, are boundary integral results for $\lambda = 100$, $Ca = Cg = 1$, □.

for a sphere approaching a deformable interface with $\lambda = 100$, $Ca = Cg = 1$ is also shown as a function of the particle position relative to the plane $z = 0$, and is seen to be quite close to the result for $\lambda = 0.0$ and $Ca = Cg = 0.01$. At first, this agreement between results for low and high viscosity ratios appears to be quite surprising. However, it can be understood by extrapolating the far-field analytical results of Yang and Leal (1984) to the case of a sphere *near a flat* interface. In particular, Yang and Leal show that the ratio of the drag on a stationary sphere near a flat interface to Stokes' drag for an unbounded fluid is

$$\text{Drag Ratio} = 1 + \sum_{n=1}^{3}\left[\frac{3}{8l}\frac{(2+3\lambda)}{(1+\lambda)}\right]^n - \frac{(1+4\lambda)}{8(1+\lambda)}\left(\frac{1}{l}\right)^3 - \frac{10}{12}\left(\frac{1}{l}\right)^3\left[\frac{3(2+3\lambda)}{8(1+\lambda)}\right] + O(l^{-4}), \quad (21)$$

(with a small algebraic error corrected). This drag ratio is plotted in Figure 9 for $\lambda = 0$ and $\lambda = 100$, and it can be seen that the result is *very* sensitive to λ, especially for $l \to -1$. On the other hand, the component of the resistance tensor K_{zz} for motion normal towards a flat, fluid interface is given by Lee et al. (1979) and Yang and Leal (1984) as

$$K_{zz} = 6\pi\left[1 + \sum_{n=1}^{3}\left[\frac{3}{8l}\frac{(2+3\lambda)}{(1+\lambda)}\right]^n - \frac{(1+4\lambda)}{8(1+\lambda)}\left(\frac{1}{\lambda}\right)^3\right] + O(l^{-4}), \quad (22)$$

and the *relative* velocity for a flat interface is given by the ratio of these two values, multiplied by the appropriate scales used in this study. Because the two expressions (Eqs. 21 and 22) exhibit very similar dependence on λ, the *ratio* becomes relatively insensitive to λ. In particular, the asymptotic solution shows essen-

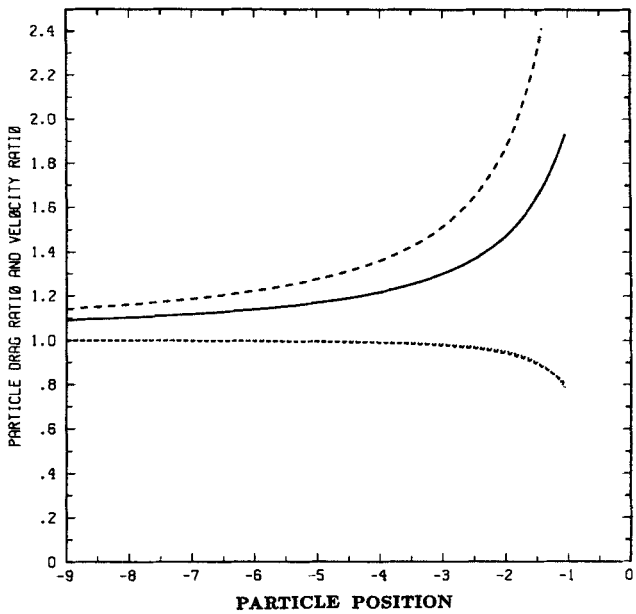

Figure 9. Particle drag ratio and relative velocity from far-field asymptotic solution.

— — —, drag for $\lambda = 0$; — — —, drag for $\lambda = \infty$; · · · · ·, velocity for $\lambda = 0$; -----, velocity for $\lambda = \infty$.

tially the same sphere velocities for large and small λ, Figure 9. The boundary integral calculations for Figures 4 and 5 exhibit a similar *insensitivity* of sphere velocity to λ. Although the far-field asymptotic solution of Yang and Leal agrees well with the bipolar coordinate solution for the drag near a flat interface (c.f. Yang and Leal, 1984), it does *not* give good agreement for the particle velocities, Figure 8. The point is that an accurate representation of the drag force is captured by the asymptotic solutions since the drag does not become singular at small separations. However, the resistance tensor, both with and without interface deformation, grows much more rapidly than the asymptotic representation as the particle/interface separation becomes small. It may also be noted from Figure 8 that particle velocities based on a flat but deforming interface are much larger than the actual particle velocities for a deformed interface.

Large Deformation Problems

Let us now turn to a more general range of values for λ, *Ca*, and *Cg*, where interface deformation does not necessarily remain small. As we have already noted, such problems find important application in evaluating surface roughness/defects in products manufactured from multiphase fluids.

The only published experimental results, so far as we know, are contained in the work of Hoffman (1985), who studied the approach of a sphere toward the free surface between two immiscible fluids that were being pumped through a circular tube. At the end of this section, we will compare the solutions obtained here with Hoffman's experimental observations. First, we attempt to understand the interface deformation problem from a more fundamental point of view, based on comparisons of solutions obtained with a systematic variation of the three dimensionless parameters, λ, *Ca*, and *Cg*.

Effect of viscosity ratio

We begin by considering the effects of variations in the viscosity ratio, λ, for fixed values of $Ca = Cg = 1$. Results for the interface shapes and relative sphere/interface position are plotted in Figures 10, 11 and 12, at equal time intervals of 0.25 for $\lambda = 0$, 1, and 10. The most obvious distinction from the preceding section is that the deformation is no longer small.

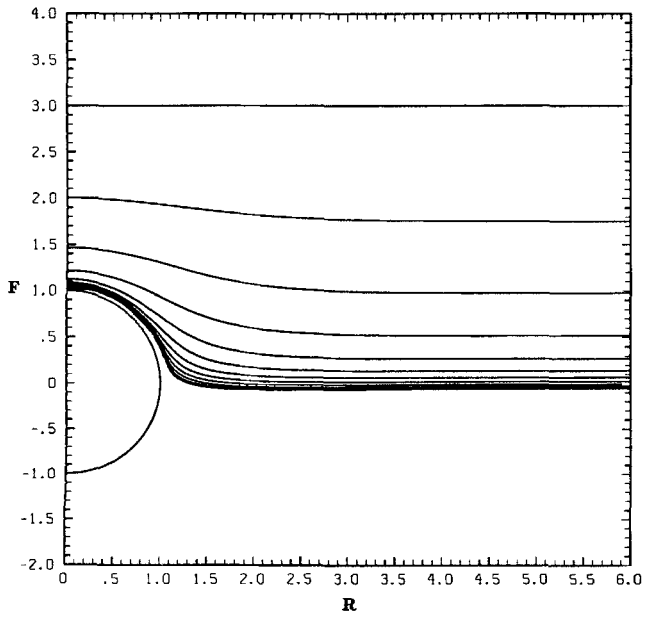

Figure 10. Interface shape as a function of sphere position: $\lambda = 0$; $Ca = Cg = 1$; $l_o = -3$; $\Delta t_c = 0.25$.

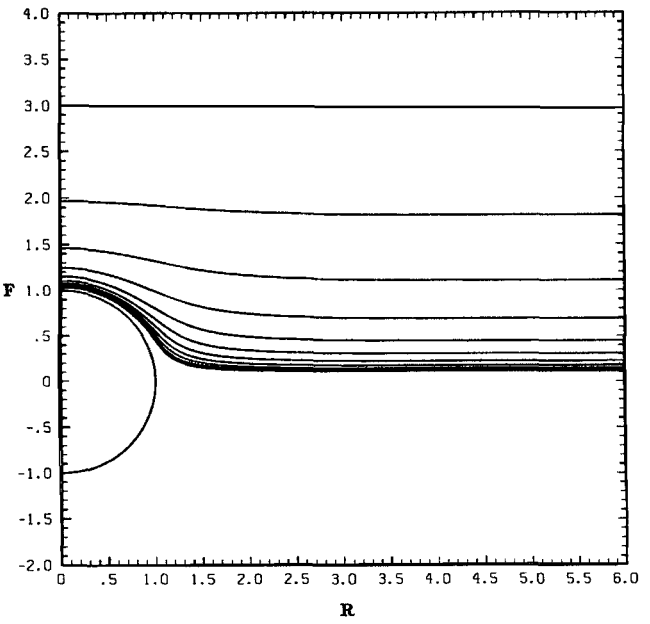

Figure 11. Interface shape as a function of sphere position: $\lambda = Ca = Cg = 1$; $l_o = -3$; $\Delta t_c = 0.25$.

Perhaps the most surprising feature of the solutions for the interface shape is that they are qualitatively insensitive to λ over the whole range $0 \leq \lambda \leq 10$. To be sure, there is a quantitative difference in the degree of deformation, with the largest deformation for the free surface $\lambda = 0$, and smaller deformation for the larger viscosity ratios. However, it is not until $\lambda = 100$, considered in the preceding section, that an increase of the viscosity

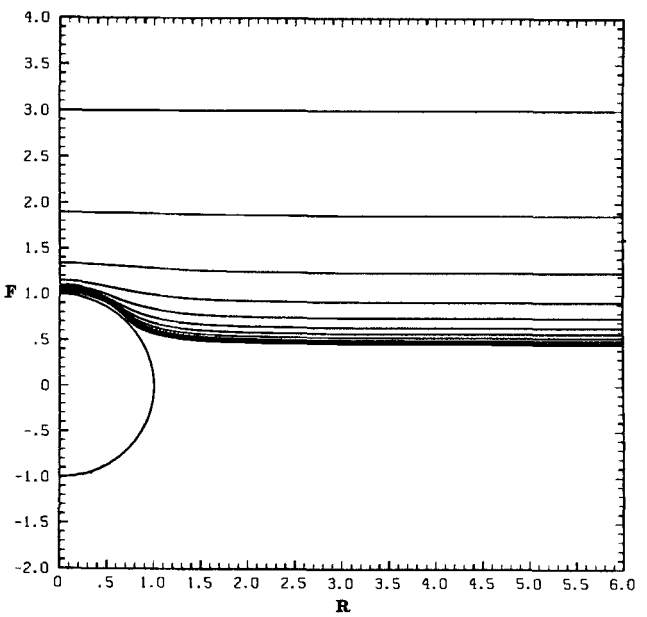

Figure 12. Interface shape as a function of sphere position: $\lambda = 10$; $Ca = Cg = 1$; $l_o = -3$; $\Delta t_c = 0.25$.

ratio produces a large reduction in the maximum degree of interface deformation. In contrast, the solutions obtained earlier by Geller et al. (1986), for motion of a sphere toward an interface under the action of a constant applied force, showed a very strong dependence of deformation on λ, and a much larger degree of deformation for equivalent values of λ, Ca, and Cg.

We have already noted three fundamental reasons for these differences in the preceding section: 1) the undisturbed velocity, and thus the driving force for particle motion, goes to zero as $l \rightarrow 0$; 2) the net force and torque on the sphere are zero and thus the disturbance flow produced is of shorter range ("weaker"); and 3) the undisturbed flow field tends to maintain the interface in a flat configuration. The manifestation of these differences between the present problem and the constant force problem of Geller et al. (1986) is pursued in some detail by Stoos (1987). Here, we concentrate on point 3), which has no counterpart in any of the interface deformation problems considered earlier.

In particular, we wish to examine the tendency, claimed above, for the undisturbed flow to maintain the interface in its undeformed state. The interface shape evolves with a net velocity, which is the sum of the disturbance velocity and the undisturbed velocity. The undisturbed velocity, u_∞, always acts to restore the interface to flat. This tendency is also reflected in the term $[6(\lambda - 1)(n \cdot i_r)i_r]$ which appears in expression 18 for the stress difference at the interface and plays the role of a third "restoring" mechanism, along with the usual mechanisms associated with interfacial tension and the density difference across the interface. The main distinction is that this contribution to the disturbance stress difference on the interface is proportional to the slope, $\partial f/\partial r$, as it appears in the determination of the normal to the interface, rather than the curvature, $\partial^2 f/\partial r^2$, for the capillary force or the relative displacement, f, for the body force effect.

Useful insight into the restoring effect associated with the undisturbed flow can be obtained by considering the hypothetical problem of a deformed interface with zero surface tension and equal fluid densities relaxing back toward a flat configuration with no particle present under the action of an extensional flow, [remove the integral over the particle surface from Eqs. 12–14, and neglect Eq. 9, and let $Ca = Cg = \infty$ (no interfacial tension and equal densities)]. The *initial* deformed interface shape for this calculation is chosen as the *final* interface shape in Figure 11. Since the contribution to the stress difference from the flow at infinity is geometry-dependent, deformations both above and below the plane of the undeformed interface are considered.

The result for $\lambda = 1$ is shown in Figure 13. In this case, Eq. 14 reduces to $u'' = 0$, and the interface simply "convects" with the local undisturbed flow as shown in Figure 13 for initial deformations both above and below the plane $z = 0$. As expected, the deformations above and below the plane $z = 0$ relax back at the same rate, and this relaxation slows as the interface becomes less deformed (longer time steps are used at the end for clarity).

The cases $\lambda = 0$ and 10 ($Ca = Cg = \infty$) are shown in Figures 14 and 15, respectively. From a qualitative physical point of view, it is obvious that the case $\lambda = c$ with deformation above the plane, $z = 0$, say, should be precisely equivalent to $\lambda = 1/c$ with the same deformation below $z = 0$. Thus, Figure 15 for $\lambda = 10$ is very similar to Figure 14 inverted. This is because $\lambda = 10$ is not too different from $\lambda = \infty$, insofar as this effect is concerned. It

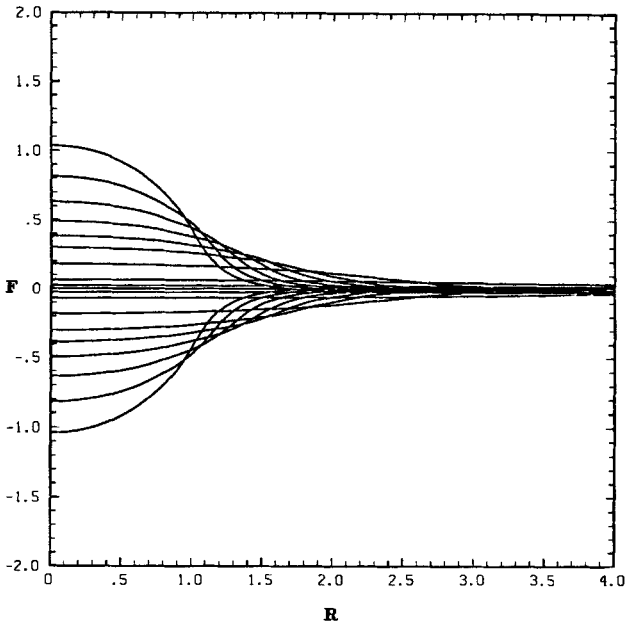

Figure 13. Shape of an initially deformed interface relaxing back to flat in the presence of an extensional flow: $\lambda = 1$; $Ca = Cg = \infty$; times = 0.0, 0.125; 0.25, 0.375, 0.50, 0.675, 0.875, 1.375, 1.875.

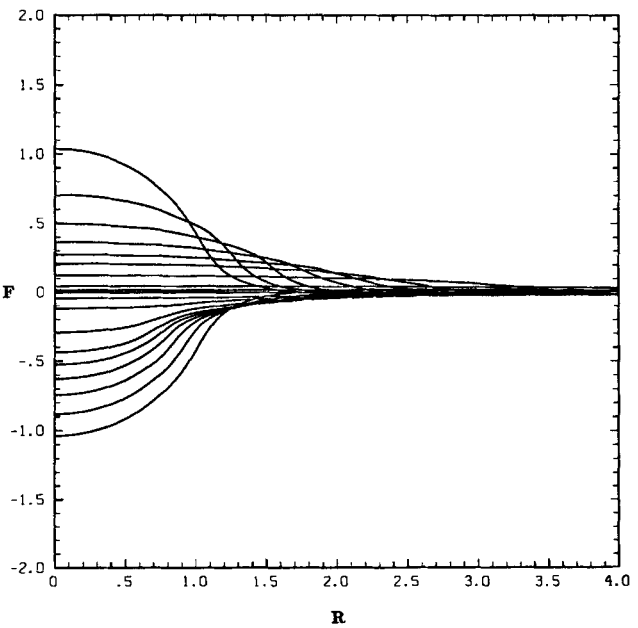

Figure 14. Shape of an initially deformed interface relaxing back to flat in the presence of an extensional flow: $\lambda = 0$; $Ca = Cg = \infty$; times = 0.0, 0.125, 0.25, 0.375, 0.50, 0.675, 0.875, 1.375, 1.875.

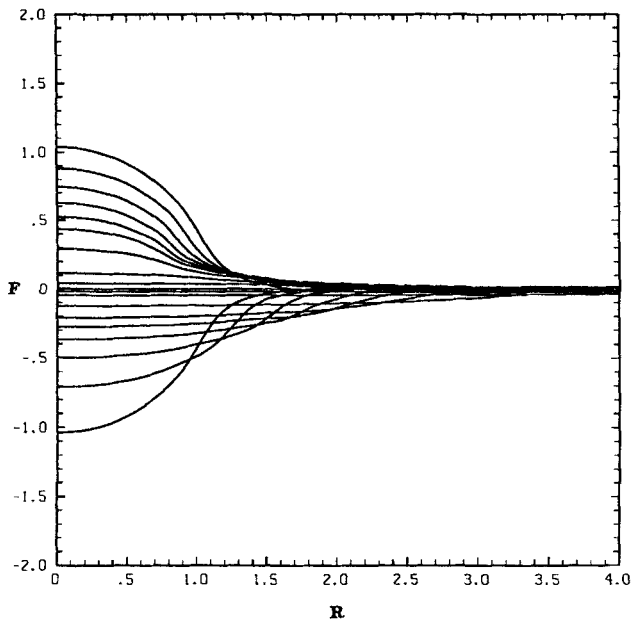

Figure 15. Shape of an initially deformed interface relaxing back to flat in the presence of an extensional flow: $\lambda = 10$; $Ca = Cg = \infty$; times = 0.0, 0.125, 0.25, 0.375, 0.50, 0.675, 0.875, 1.375, 1.875.

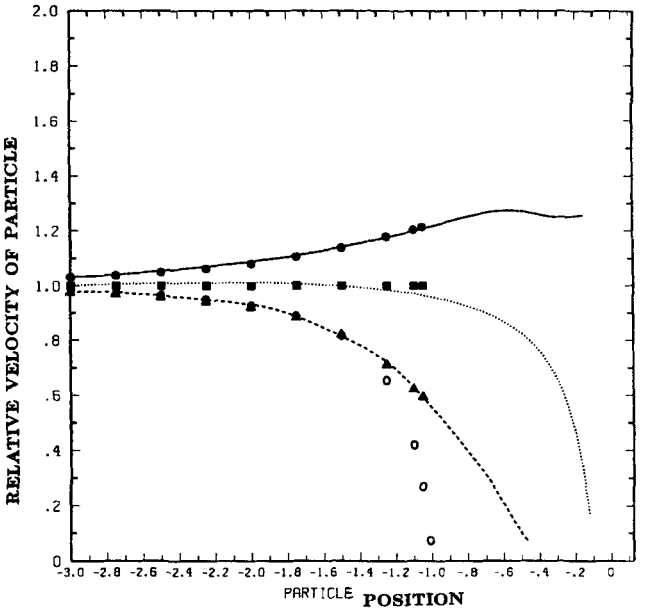

Figure 16. Relative velocity of the particle as a function of particle position.

———, $\lambda = 0$, $Ca = Cg = 1$; -----, $\lambda = 10$, $Ca = Cg = 1$; · · · · ·, $\lambda = 1$, $Ca = Cg = 1$; □, boundary integral solution for a flat but deforming interface with $\lambda = 1$, $Ca = Cg = 1$; Δ, boundary integral solution for a flat but deforming interface with $\lambda = 10$, $Ca = Cg = 1$; O, boundary integral solution for a flat but deforming interface with $\lambda = 0$, $Ca = Cg = 1$; O, bipolar coordinate solution for a flat interface with $\lambda = 0$.

may be noted that the last term in Eq. 18 changes sign for deformations above or below $z = 0$, and also for λ greater than or less than unity. This produces an asymmetry in the relaxation process. For positive values of $6(\lambda - 1)(n \cdot i_r)$, this term in the stress balance tends to reduce the slope of the interface deformation by forcing the deformed part of the interface toward $r = 0$, as in the bottom part of Figure 14 and the top part of Figure 15. For negative values of $6(\lambda - 1)(n \cdot i_r)$, this term in the stress balance tends to reduce the slope of the interface deformation by pushing the deformed part of the interface out towards $r = \infty$, as in the top part of Figure 14 and the bottom part of Figure 15. Thus, for the particle approach problems (Figures 10–12), a principal effect of the $6(\lambda - 1)(n \cdot i_r)$ term in the stress balance will be to concentrate the deformation near $r = 0$ for larger λ, and this may account in part for the pinching of the interface on the shoulder of the particle for $\lambda = 10$, Figure 12.

As important as the qualitative shape of the interface is the *rate* of deformation and its dependence upon λ. It can be examined by investigating the particle velocities as a function of position and λ.

The calculated particle velocities relative to the velocity of the undisturbed flow field at the particle center ($u_p/-2l$) are shown in Figure 16 as a function of particle position (the actual particle velocities for $Ca = 1$, Cg, and λ between 0.1 and 10.0 can be found in Stoos, 1987). Also shown in Figure 16 are the relative particle velocities that would occur for the same fluid if the interface were flat but deforming (i.e., $u \cdot n \neq 0$), and the bipolar coordinate predictions of Dukhin and Rulev for a flat *nondeforming* interface (i.e., $u \cdot n = 0$) with $\lambda = 0$. The most surprising result from Figure 16 is that the relative particle velocities for the deformed interface solutions are matched almost perfectly by the predictions for a flat but deforming interface all the way up to $l \approx -1$, in spite of the fact that the interface becomes quite deformed before that point. There is no simple explanation for this observation. In all three cases, the interface deforms prior to $l = -1$, and one would expect interfacial tension and the density difference to begin to play a role, which could not be duplicated by the results for a flat interface. The fact that the particle velocity does not deviate significantly from the results for a flat but deforming interface, as it does for $Ca = Cg = 0.01$, $\lambda = 0$ in Figure 8, must reflect the presence of other compensating factors. Among these is the fact that the deformed interface lies farther from the sphere, thus reducing the importance of direct hydrodynamic interactions ("wall effects"). In addition, the hydrodynamic driving force for motion of the sphere is increased for $\lambda = 0$ and decreased for $\lambda = 10$ via the modification in the flow field that is necessary to accommodate interface deformation. Another puzzling feature of Figure 16 is that the predictions from the bipolar coordinate solution for a flat interface with $\lambda = 0$ that is *not* deforming (i.e., $u \cdot n = 0$) give particle velocities that actually agree most closely with the numerical predictions for $\lambda = 10$! The latter behavior is most likely related to the agreement we saw earlier between particle velocities for $\lambda = 0$ and 10 for the small deformation case, since in the "large" deformation case, the deformation is not really large for $\lambda = 10$ until $l \geq -1$. This is a result of the effect of the flow field itself restoring the interface to flat for large λ.

Finally, it is interesting to note that the particle velocity for $\lambda = 0$ is *larger* than that if the particle simply convected along with the undisturbed flow. This is further evidence (along with the increase in drag) of the modification of the flow field resulting from the interface deformation: i.e., both the particle and fluid velocities are increased in the presence of the deformed interface from the values they would have in an unbounded

fluid. It is noteworthy in this regard that the velocity of a sphere near a *flat* but deforming interface for $\lambda = 0$ is also increased over the value the *undisturbed* velocity would have at the particle center. It is important to note that it is only the *relative* velocity of the sphere that may *increase* as the distance from the interface gets smaller for $\lambda \ll 1$. Figure 17 shows that the actual particle velocity decreases monotonically as the sphere approaches the interface for all values of λ! (cf., Figure 25).

Two quantitative measures of the degree and rate of deformation are the minimum gap width between the sphere and the interface, and the maximum displacement (or penetration) of the interface from the plane $z = 0$. These two quantities are plotted in Figure 17 as a function of the position of the sphere and in Figure 18 as a function of time. The minimum gap width is always smallest at a given sphere position for the largest value of λ, Figure 17. More noticeable, in Figure 18, is the fact that the interface for $\lambda = 10$ is displaced very little until the sphere is very close to the plane of the undeformed interface: essentially this lack of significant deformation is the reason why the minimum gap width is smaller for $\lambda = 10$. In a practical context, either in terms of the potential to produce a significant bump on the interface or in terms of capture efficiencies in separation processes, it is more interesting to examine the minimum gap and the penetration depth as a function of time (recall that the motion toward the interface due to the axisymmetric stagnation component of a bulk flow is usually only one component of the particle trajectory, which also carries the particle parallel to the plane of the undeformed interface and thus allows only a finite *time* for interface deformation; Stoos, 1987). Examining Figure 18, we see that neither the rate of thinning of the gap nor the rate of increase in the displacement of the interface is a very strong function of λ, at least in the range $0 \leq \lambda \leq 10$ that is considered in this section. This is especially true at large times where the dynamics of "film drainage" takes over and the rate of thinning of the film becomes surprisingly invariant to changes in λ.

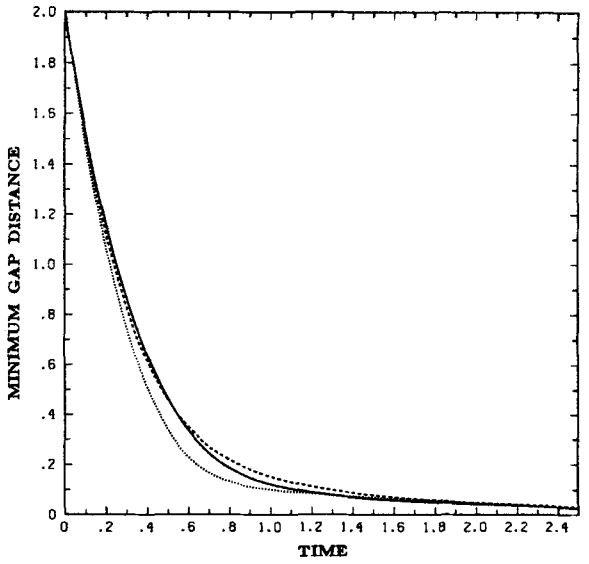

Figure 18. Minimum particle-interface separation distance as a function of time: *Ca* = *Cg* = 1: — — —, $\lambda = 0$; · · · · ·, $\lambda = 1$; ——, $\lambda = 10$.

One additional comparison with earlier work, which is of some interest, is the fact that the shape of the thin film appears to be qualitatively different from the predictions of Geller et al. (1986) for motion of a solid sphere toward the interface, and of Chi and Leal (1988), who considered the closely related problem of the motion of a drop of fluid A toward an interface separating the suspending fluid B from a large additional "body" of fluid A. In the latter case, Chi and Leal found that the shape of the thin film depended strongly on the viscosity ratio, λ, i.e.,

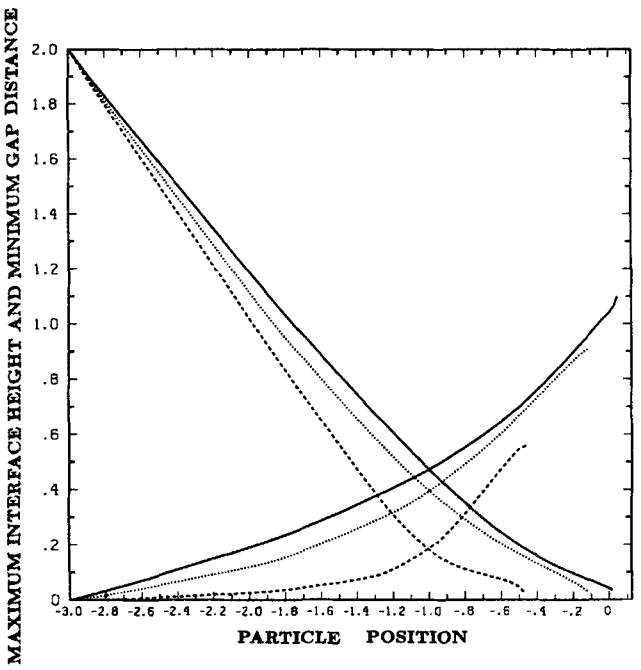

Figure 17. Maximum interface height above the plane $z = 0$ and minimum particle-interface separation distance as a function of particle position.
Ca = *Cg* = 1: ———, $\lambda = 0$; · · · · ·, $\lambda = 1$; – – – –, $\lambda = 10$.

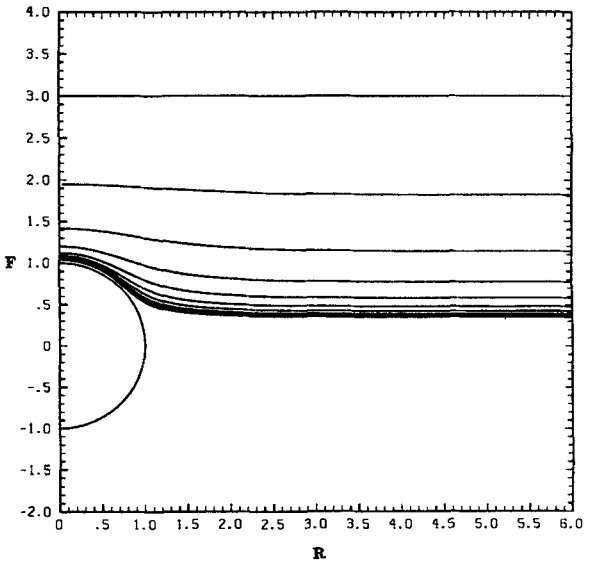

Figure 19. Interface shape as a function of sphere position: $\lambda = 1$; *Ca* = 0.1; *Cg* = 1; $l_o = -3$; $\Delta t_c = 0.25$.

μ_A/μ_B. In the present problem, the smallest particle-interface separation occurs on the axis of symmetry for both $\lambda = 0$ and 1, suggesting that if breakthrough ultimately occurs in these cases, it would occur initially at this point. In contrast, all of the previous studies had shown that the minimum film thickness occurred away from the axis (as in the present problem for $\lambda = 10$) if either the particle was solid or the drop viscosity was large, and the previous authors had tentatively concluded that the film on a solid sphere would always have a minimum thickness at an off-axis position. Clearly, however, the present results show that this is not the case, and the film geometry is a subtle function of the undisturbed flow and the material parameters.

Effect of surface tension and gravity forces

Let us now turn to the effects of surface tension forces, i.e., *Ca*, and/or the density difference, as measured by *Cg*, in determining the nature and magnitude of interface deformation. For this purpose, we have considered $Ca = 0.1$, 1, and 10 with $Cg = 1$ for $\lambda = 0$, 1, and 10, as well as $Cg = 0.1$, 1, and 10 with $Ca = 1$ and $\lambda = 0$, 1, and 10. The majority of the particle/interface configurations for these solutions are similar to those already presented in Figures 10-12. The reader may refer to Stoos (1987) for detailed interface shapes for cases that are not given here. The overall conclusion is that the deformation is remarkably insensitive to *Ca* and *Cg* for $\lambda \geq 1$. However, some discussion of the cases not shown is important.

For $\lambda = 10$, the interface configuration was essentially independent of *Ca* and *Cg* over the whole range from $0.1 \leq Ca, Cg \leq 10$, with the results being very similar to the case $Ca = Cg = 1$, $\lambda = 10$ that was shown in Figure 12. For $\lambda = 1$, the results for $Ca = 10$, $Cg = \lambda = 1$, and $Cg = 10$, $Ca = \lambda = 1$ are virtually identical with the case $Ca = Cg = \lambda = 1$ that was presented in Figure 11. Since *Ca* and *Cg* represent different mechanisms that act to inhibit deformation in a qualitatively different way, the fact that the interface shape does not change upon increase of *Ca* or *Cg* can be explained only by the fact that the deformation is dominated by viscous effects even for $Ca = Cg = \lambda = 1$. Hence, for $\lambda \geq 1$, the potential for controlling the magnitude of interface deformation by variation of *Ca* or *Cg* is rather limited in the sense that very small values of *Ca* or *Cg* must be required, as will be discussed in the next section.

Only for *Ca* or $Cg = 0.1$ is a significant change in the interface shape observed for $\lambda = 1$. Results corresponding to the two cases $Ca = 0.1$, $Cg = \lambda = 1$ and $Cg = 0.1$, $Ca = \lambda = 1$ are shown in Figures 19 and 20, respectively. In these cases, the degree of deformation is significantly reduced relative to $Ca = Cg = \lambda = 1$ (Figure 11). Furthermore, the active roles of interfacial tension and the density difference in determining the interface shape is reflected in the *differences* in the details of the interface shapes shown in Figures 19 and 20. The interface shape in the latter case is similar to the shapes seen earlier, with the minimum film thickness occurring at the symmetry axis, and the interface contour following the particle shape quite closely until a relatively sharp break occurs in the transition to the undeformed flat interface. On the other hand, the magnitude of deformation is smaller in Figure 19 and there is a smoother, broader shape with no regions of high interface curvature in the transition to the undeformed shape. One consequence of the restriction on curvature is that the minimum film thickness no longer occurs at the symmetry axis. Indeed, the interface shapes in Figure 19 more closely resemble the interface shapes in Figure 12, which correspond to $\lambda = 10$, $Ca = Cg = 1$, pointing up again the complicated dependence of the film geometry on the flow and material parameters.

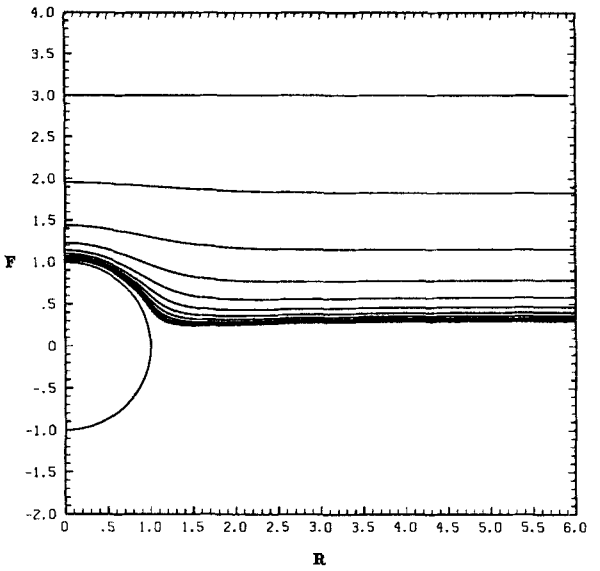

Figure 20. Interface shape as a function of sphere position: $\lambda = 1$; $Ca = 1$; $Cg = 0.1$; $l_o = -3$; $\Delta t_c = 0.25$.

Results were also obtained for $\lambda = 0$, with various values of *Ca* and *Cg* in the range $0.1 \leq Ca \leq 10$ and $0.1 \leq Cg \leq 10$. Not surprisingly, the interface shapes for $\lambda = 0$ were relatively more sensitive to *Ca* and *Cg*. Most of the results are not reproduced here (see Stoos, 1987). We show only a few selected cases for "small" values of *Ca* and/or *Cg*.

In particular, in Figure 21, we show the interface shapes for the case $Ca = Cg = 0.1$, $\lambda = 0$, which may be compared with Figures 4 and 10 where $Ca = Cg = 0.01$ and $Ca = Cg = 1$, respectively. It is clear that the effectiveness of the flow field in

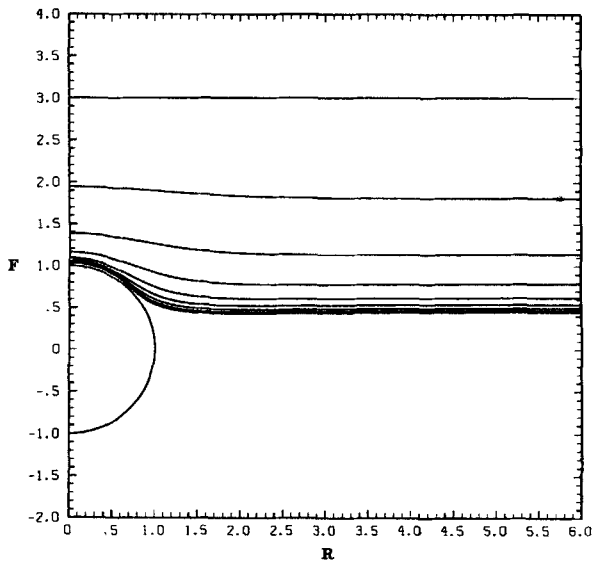

Figure 21. Interface shape as a function of sphere position: $\lambda = 0$; $Ca = Cg = 0.1$; $l_o = -3$; $\Delta t_c = 0.25$.

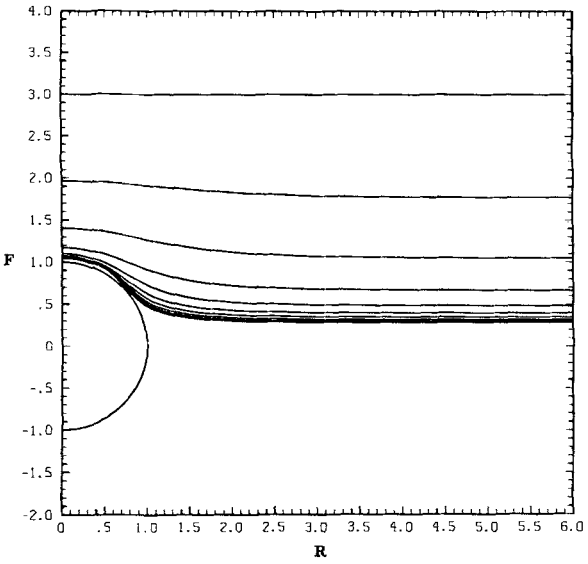

Figure 22. Interface shape as a function of sphere position: $\lambda = 0$; $Ca = 0.1$; $Cg = 10$; $l_o = -3$; $\Delta t_c = 0.25$.

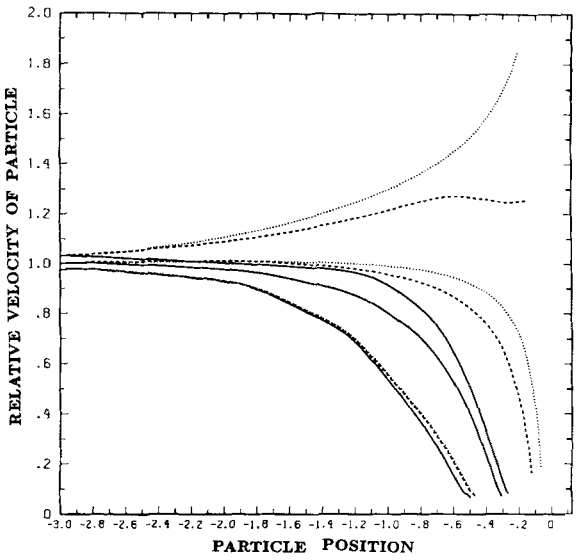

Figure 24. Relative velocity of the particle as a function of particle position.

$\lambda = 0$, 1, and 10, $Ca = 1$: ———, $Cg = 0.1$; -----, $Cg = 1$; · · · · ·, $Cg = 10$.

"resisting" deformation does not dominate the effects of changes in Ca and Cg for $\lambda = 0$ as it does for $\lambda = 1$ and 10. Further, the transition between moderate and very small interface deformation can be seen to occur for Ca and Cg between 0.1 and 0.01. We shall return to this point shortly.

To isolate the effects of high surface tension and large density differences, the results in Figures 22 and 23 show solutions where either Ca or Cg is small while the other is large (while still maintaining $\lambda = 0$). Thus, Figure 22 shows results for $Ca = 0.1$, $Cg = 10$, and $\lambda = 0$, and Figure 23 shows results for $Ca = 10$, $Cg = 0.1$, and $\lambda = 0$. It can be seen that the interface shapes with capillary forces dominating ($Ca = 0.1$, $Cg = 10$, and $\lambda = 0$) are considerably different from the interface shapes with gravity effects dominating ($Ca = 10$, $Cg = 0.1$, and $\lambda = 0$), and both show more deformation than for $Ca = Cg = 0.1$, Figure 21. With surface tension dominant, there is again a smooth interface shape with no region of high interface curvature in the transition region. The interface deformation is somewhat larger than for $Ca = Cg = 0.1$ in Figure 21 and the existence of a minimum film thickness off the axis is accentuated for this case. Indeed, the separation between the sphere and the interface on the axis is still quite large at the point where the minimum gap width becomes so small that the calculation had to be stopped. On the other hand, for a dominant gravitational restoring force, i.e., for $Ca = 10$, $Cg = 0.1$, and $\lambda = 0$, as shown in Figure 23, the interface has large localized curvature in the transition region to a flat interface. In fact, for this case, the interface height actually dips slightly below the plane $z = 0$. Thus, although the amplitude of the "bump" produced relative to the undeformed interface is the same magnitude as in the case $Ca = 0.1$, $Cg = 10$, the appearance is of a larger distortion of the interface shape. This slight interface depression seems to result from the larger downward tangential velocity that occurs when the heavy lower fluid, which has been forced above the plane $z = 0$, drains from the top of the sphere. This interface depression occurs only after the sphere velocity has decreased to near zero (≥ 0.05 from an initial velocity of 6.2); thus, the velocity field in this region is dominated by the drainage flow rather than by the flow resulting from the motion of the sphere. It should also be noted that this interface depression does not occur for $\lambda = 1$, or 10. Finally, the minimum separation distance between the interface and the sphere occurs on the axis of symmetry in Figure 23, although the separation is quite small over the entire top of the sphere as the heavy fluid trapped there drains away.

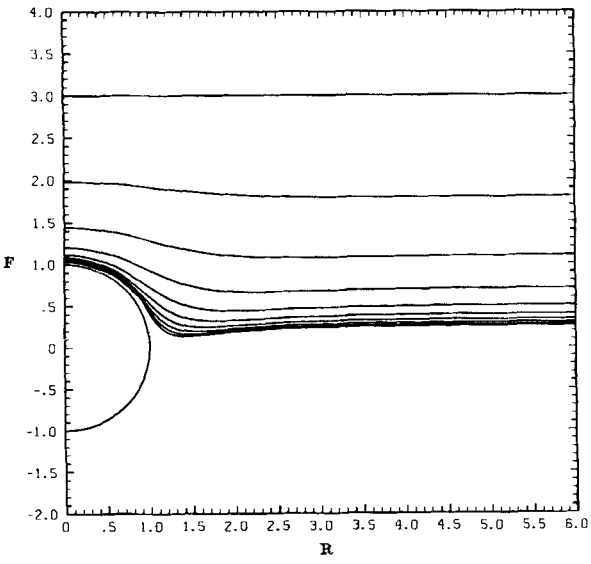

Figure 23. Interface shape as a function of sphere position: $\lambda = 0$; $Ca = 10$; $Cg = 0.1$; $l_o = -3$; $\Delta t_c = 0.25$.

Although the interface shapes are relatively insensitive to variations in the *nondominant* parameter (i.e., we found virtually identical shapes for $Ca = 10$, $Cg = \lambda = 1$; and $Cg = 10$, $Ca = \lambda = 1$, and $Ca = Cg = \lambda = 1$), the particle velocity is sensitive to changes in this parameter, as is seen in Figures 24 and 25 where the relative particle velocities for $Ca = 1$ and $0.1 \geq Cg \leq$

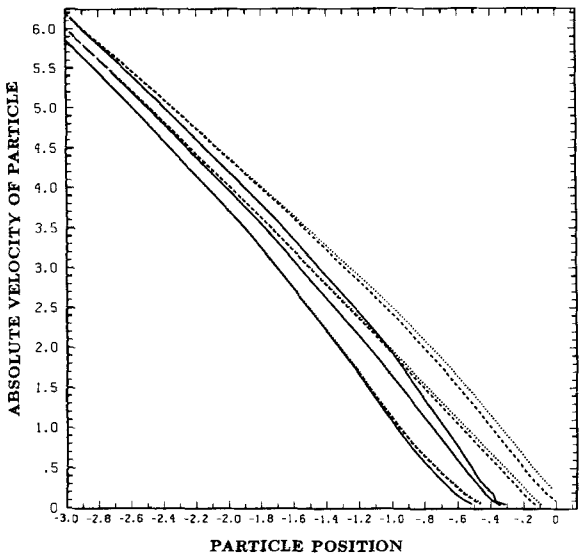

Figure 25. Absolute velocity of the particle as a function of particle position.

$\lambda = 0$, 1, and 10, $Cg = 1$: ———, $Ca = 0.1$; -----, $Ca = 1$; · · · · ·, $Ca = 10$.

10 and the absolute particle velocities for $Cg = 1$ and $0.1 \geq Ca \leq 10$ are plotted, respectively. The corresponding plots for relative particle velocities with $Cg = 1$ and absolute particle velocities with $Ca = 1$ show qualitatively similar behavior (with Cg and Ca switched) and thus are not shown. From Figure 24, it is clear the relative particle velocity is sensitive to changes in Ca and Cg except when $\lambda = 10$, in which case viscous effects dominate and the particle velocity is insensitive to variations in Ca and Cg. Small values of Ca and Cg are less dominant in controlling the particle velocity: e.g., there is still considerable variation in particle velocity with λ for $Cg = 0.1$ (and also $Ca = 0.1$). One noticeable feature of Figure 24 is the rapid increase in the relative particle velocity for $\lambda = 0$, $Cg = 10$ as the particle center approaches the plane $z = 0$. This behavior is merely a consequence of the fact that the particle has a finite velocity as it passes this plane, while the scaling factor $(-u_p/21)$ blows up.

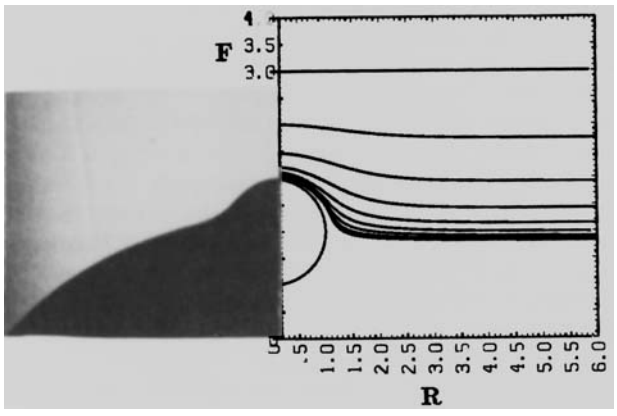

Figure 26. Interface shape as a function of sphere position: $\lambda = 0$; $Ca = 44$; $Cg = 49$; $l_o = -3$; $\Delta t_c = 0.25$. Also shown is the experimental results of Hoffman (1985) for this case.

The actual particle velocity decreases monotonically as the particle approaches the interface, Figure 25.

Magnitude of surface bumps

One of the primary motivations for interest in the motion of particles carried by a mean flow toward a fluid interface is the problem of surface bumps or imperfections that may be a consequence of the deformation produced by small particles during a manufacturing process that involves a flow (mold filling, for example). This aspect was studied by Hoffman (1985), as indicated in the introduction, and we use this final section of "results" for a brief comparison with his work, as well as for a summation of our predictions of the magnitude of interface deformation vs. the dimensionless parameters λ, Ca, and Cg. The problem considered experimentally by Hoffman corresponds to the final remaining case of interest, with Ca and Cg both large and $\lambda = 0$. To compare with the experimental results from Figure 12c in Hoffman (1985), calculations are performed for a particle approaching a deformable interface in an extensional flow with $Ca = 22.07$, $Cg = 24.34$, and $\lambda = 0$. [The tube in Hoffman's experiment was horizontal, rather than vertical. However, for $Cg \geq 0(1)$ with $\lambda = 0$, gravitational effects should be negligible in any case.] This figure from Hoffman is chosen because the particle appears to be near the axis of the tube, and thus the variation of the extensional flow strength with the position in the tube can be neglected: i.e., if the position in the tube is specified by the angle θ_E, defined by Hoffman, it is assumed $\theta_E = 0$. The shape of the interface calculated numerically is shown in Figure 26 along with Hoffman's original photograph. The calculated shape is quite similar to that obtained experimentally, although the numerics predict a somewhat larger maximum interface deformation.

It should be kept in mind, however, that Hoffman's photo is just a representative sample of the bumps produced and is not claimed by Hoffman to be at a maximum deformation magnitude. The maximum heights of the deformed interface above the plane $z = 0$ are given for all the systems considered by Hoffman in his Figure 11. The maximum deformation in the numerical solution in Figure 26 is approximately 0.75 (based on particle diameter) compared to 0.67 (based on particle diameter) from Figure 11 of Hoffman. The fact that there is some disagreement between the maximum deformation given by the numerics and by the experiments may be due to the finite curvature present in the experimental fluid front, which will affect both the flow field and the tendency of the interface to deform. Also, the asymmetry inherent in the experiments for particles that are off the tube axis may account for some of the scatter in the results in Hoffman's Figure 11. Other detailed comparisons are not possible because experimental difficulties make it impossible to determine the particle position in Hoffman's experiments. However, in a general sense, the agreement with Hoffman's experimental results appears to be good.

The final flow characteristic investigated is the maximum interface deformation for: viscosity ratios of 0.0, 1.0, and 10.0; capillary numbers of 0.1, 1.0, and 10.0; and Cg of 0.1, 1.0, and 10.0. Also, for completeness, the maximum interface deformation for the limiting cases of small deformation, i.e., $Ca = Cg = 0.01$, $\lambda = 0$ and $Ca = Cg = 1$, $\lambda = 100$, are considered also. For the interface shapes for the parameter values that were not presented earlier, see the cases in Stoos (1987). Figure 27 shows the maximum interface deformation (maximum distance of the

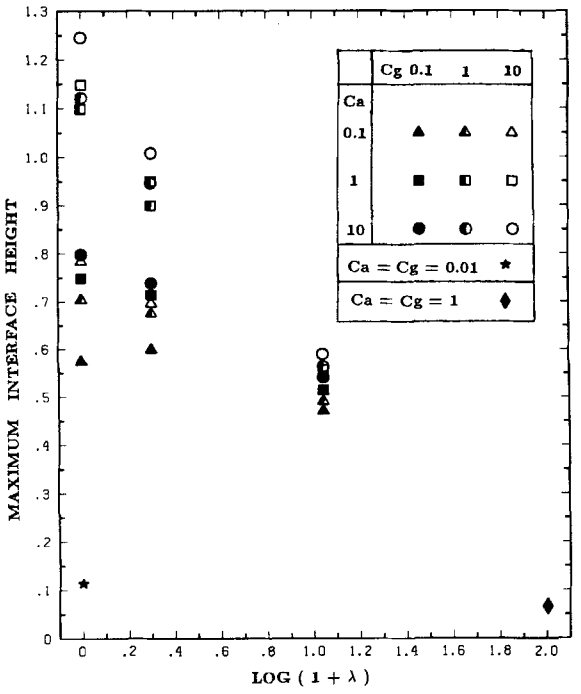

Figure 27. Maximum interface deformation as a function of λ for all values of *Ca* and *Cg* considered.

interface from the plane $z = 0$) for the above parameters. The most noticeable feature of this plot is the drastically decreased sensitivity of the deformation magnitude on *Ca* and *Cg* for increasing viscosity ratios. Viscous effects, from the undisturbed flow, control the deformation magnitude for large λ, and the effects of variations in *Ca* and *Cg* on the deformation are small.

Thus, to maintain a bump size of 0.6 particle radii or less for small viscosity ratios, the operating conditions (processing speed) must correspond to *Ca* and $Cg = 0.1$ or less. On the other hand, for viscosity ratios $\lambda \geq O(10)$, *Ca* and *Cg* can be much larger without leading to larger deformations. To limit the deformation to a small percentage of the sphere size (≤10%), however, *Ca* and *Ca* must be O(0.01) or smaller or λ must be O(100) or larger. In attempting to partially control the degree of deformation, it would be useful to note that the variation in the deformation magnitude is much larger when decreasing *Ca* or *Cg* from 1.0 to 0.1 than when decreasing *Ca* or *Cg* from 10.0 to 1.0. Indeed, for many cases it appears that values of *Ca* or *Cg* of O(1) behave like *Ca* and $Cg \gg 1$. Also, it appears that surface tension is somewhat more effective in decreasing the maximum deformation than are density differences. The smallest deformations are found for the smallest values of *Ca* ($Ca = 0.1$, $Cg = 1.0$ always has smaller deformation than $Cg = 0.1$, $Ca = 1.0$).

Conclusions

Many characteristics of the interface deformation and particle velocity profiles for a sphere driven towards a deformable interface by a biaxial extensional flow are qualitatively similar to what has been observed for spheres and drops approaching a deformable interface at a constant velocity or under the action of a constant external force, e.g., gravity. For example, this is true of the qualitative changes associated with variations in λ, *Ca*, and *Cg*. However, interfacial tension and/or the density difference across the interface play a dominant role in determining the degree and nature of interface deformations only for *Ca*, $Cg \leq O(0.01)$, and thus the viscosity ratio remains as the dominant factor even for *Ca*, $Cg = O(1)$. This may be contrasted with the results of earlier studies where the interfacial tension and density difference play a dominant role for *Ca*, $Cg = O(1)$. It may also be noted, in the present case, that the size and shape of the interface deformations agree reasonably well with the experimental results of Hoffman for large values of *Ca* and *Cg*, and the sphere velocities are in good agreement with bipolar coordinate solutions for very small deformations.

In addition, many detailed characteristics of the interface deformation are different from the previous cases and yield surprising results for some particular applications. In general, interface shapes in the presence of the flow field are flatter, with the deformation more localized near the sphere when compared to the constant velocity or constant force cases, because the undisturbed flow field itself tends to maintain the interface flat. Hence, through the interaction of the viscosity ratio with the flow field, the "viscous" effects play a role in addition to controlling the rate of thinning of the fluid in the gap as in the constant force problem. Consequently, variations in λ have a large effect on interface deformation and sphere velocity. Since the flow itself tends to keep the interface flat, broad, small-scale deformations are not seen for small *Ca* (the flow damps these out quickly) as was characteristic of the small *Ca* behavior for particle motion at a constant velocity or because of a constant force. Rather, *Ca* influences the total amount of deformation primarily by controlling the curvature in the transition region between the sphere and the undeformed interface. Also, since the disturbance caused by the sphere is more rapidly decaying than the point force disturbances associated with the constant velocity and constant force cases, the variation of the sphere velocity resulting from hydrodynamic interaction with the interface is weaker.

The effect of interface deformation may be important in polymer processing operations. To aid in estimating the size of possible interface deformations, Figure 27 summarizes the dependence of the maximum interface deformation on the operating parameters *Ca*, *Cg*, and λ.

Acknowledgement

This work was sponsored by a grant from the Fluid Mechanics program at NSF.

Literature Cited

Berdan, C., and L. G. Leal, "Motion of a Sphere in the Presence of a Deformable Interface: I. Perturbation of the Interface from Flat: the Effects on Drag and Torque," *J. Colloid Interf. Sci.*, **87**, 62 (1982).

Chi, B., and L. G. Leal, "A Theoretical Study of the Motion of a Viscous Drop toward a Fluid Interface at Low Reynolds Number," *J. Fluid Mech.*, to appear (1989).

Chwang, A. T., and T. Y-T. Wu, "Hydrodynamics of Low-Reynolds Number Flow: 2. Singularity Method for Strokes Flows," *J. Fluid Mech.*, **67**, 787 (1975).

Derjaguin, B. V., and S. S. Dukhin, "Kinetic Theory of the Flotation of Fine Particles," *Proc. of Int. Mineral Process. Cong.*, Elsevier, Amsterdam (1981).

Dobby, G. S., and J. A. Finch, "A Model of Particle Sliding Time for Flotation Size Bubbles," *J. Colloid Int. Sci.*, **109**, 493 (1986).

Dukhin, S. S., and N. N. Rulev, "Hydrodynamic Interaction between a Solid Spherical Particle and a Bubble in the Elementary Act of Flotation," *Colloid J. USSR*, **39**, 270 (1977).

Fritch, L., "Injection-Molding ABS? Mold in Quality with the Machine," *Plastics Eng.*, **35**(5), 68 (1979).
Geller, A. S., S. H. Lee, and L. G. Leal, "The Creeping Motion of a Spherical Particle Normal to a Deformable Interface," *J. Fluid Mech.*, **169**, 27 (1986).
Hoffman, R. L., "Response of a Rigid Sphere to an Extensional Flow Field Near a Liquid-Gas Interface," *J. of Rheol.*, **29**(5), 579 (1985).
Jameson, G. J., S. Nam, and M. M. Young, "Physical Factors Affecting Recovery Rates in Flotation," *Minerals Sci. Eng.*, **9**, 103 (1977).
Jeffreys, G. V., and G. A. Davies, *Recent Advances in Liquid/Liquid Extraction,* ed., C. Hanson, Pergamon Press, New York, 495 (1971).
Lee, S. H., R. S. Chadwick, and L. G. Leal, "Motion of a Sphere in the Presence of a Plane Interface: 1. An Approximate Solution by Generalization of the Method of Lorentz, "*J. Fluid Mech.*, **93**, 705 (1979).
Lee, S. H., and L. G. Leal, "Motion of a Sphere in the Presence of a Deformable Interface: 2. Numerical Study of the Translation of a Sphere Normal to an Interface," *J. Colloid Int. Sci.*, **87**, 81 (1982).
Rallison, J. M., and A. Acrivos, "A Numerical Study of the Deformation and Burst of a Viscous Drop in an Extensional Flow," *J. Fluid Mech.*, **89**, 191 (1978).
Ruschak, K. J., "Coating Flows," *Ann. Rev. Fluid Mech.*, **17**, 65 (1985).
Smith, P. G., and T. G. M. Van de Ven, "The Effect of Gravity on the Drainage of a Thin Liquid Film between a Solid Sphere Interface and a Liquid/Fluid Interface," *J. Colloid Interf. Sci.*, **100**, 456 (1984).
Stoos, J. A., Ph.D., diss., California Institute of Technology (1987).
Yang, S.-M., and L. G. Leal, "Particle Motion in Stokes Flow near a Plane Fluid-Fluid Interface: 2. Linear Shear and Axisymmetric Straining Flows," *J. Fluid Mech.*, **149**, 275 (1984).
Youngren, G. K., and A. A. Acrivos, "Stokes Flow Past a Particle of Arbitrary Shape: A Numerical Method of Solution," *J. Fluid Mech.*, **69**, 377 (1975).
Youngren, G. K., and A. A. Acrivos, "On the Shape of a Gas Bubble in a Viscous Extensional Flow," *J. Fluid Mech.*, **76**, 433 (1976).

Manuscript received on Sept. 22, 1988 and revision received Aug. 19, 1988.